Journal of Nuclear Materials 479 (2016) 338–346

Contents lists available at ScienceDirect

Journal of Nuclear Materials

journal homepage: www.elsevier.com/locate/jnucmat

Kinematic hardening in creep of Zircaloy

Radan Sedláček*, Dietmar Deuble

AREVA GmbH, Paul-Gossen-Str. 100, 91052, Erlangen, Germany

ARTICLE INFO

Article history:
Received 6 April 2016
Received in revised form
22 June 2016
Accepted 9 July 2016
Available online 11 July 2016

ABSTRACT

Results of biaxial creep tests with stress changes on Zircaloy-2 tube samples are presented. A Hollomon-type viscoplastic strain hardening model is extended by the Armstrong-Frederic nonlinear kinematic hardening law, resulting in a mixed (i.e. *isotropic* and *kinematic*) strain hardening model. The creep tests with stress changes and similar tests published in the literature are simulated by the models. It is shown that introduction of the kinematic strain hardening in the viscoplastic strain hardening model is sufficient to describe the creep transients following stress drops, stress reversals and stress removals.

1. Introduction

Kinematic hardening is an increase in flow stress in the course of plastic deformation. As distinct from isotropic hardening, the flow stress decreases upon load reversal. The latter phenomenon is also known as the Bauschinger effect. In terms of continuum plasticity, the isotropic hardening corresponds to a yield surface extension, whereas the kinematic hardening is related to a yield surface translation in the stress space.

It is well known that kinematic hardening and Bauschinger effect occur in plastic deformation of Zircaloy. Strain control, tension/compression tests at room temperature conducted on unirradiated Zircaloy-2 specimens revealed strong kinematic hardening and Bauschinger effect [1,2]. A strong Bauschinger effect was reported also in cyclic stress-strain response of unirradiated and irradiated Zirconium alloys at elevated and room temperature, e.g. Refs. [3–5]. Hardening relaxation/unloading tests on unirradiated and irradiated Zirconium alloys at elevated temperature also confirmed the occurrence of the Bauschinger effect [4,6].

The occurrence of kinematic hardening and Bauschinger effect in Zirconium alloys has been interpreted at the microscopic scale as follows: The limited number of slip systems in the hexagonal crystallographic structure of α-Zirconium results in a pronounced anisotropy of single crystal plastic deformation. When a polycrystalline aggregate is subject to an increasing load, the grains with slip systems favorably orientated for easy activation by the load will begin to deform plastically first. Other grains whose slip systems have not yet been activated will respond to the load elastically. To maintain the strain compatibility in the aggregate, the difference in plastic strains among grains must be accommodated elastically. In this way, the intergranular deformation incompatibilities lead to buildup of internal stresses.[1] The evolving internal stresses oppose the deformation during prestrain, and favor it upon load reversal. The evolution of internal stresses in plastically deforming Zircaloy were confirmed experimentally by in situ neutron diffraction measurements [7].

In mathematical modeling of plasticity, one can account for the internal stresses and their effect on deformation behavior at different levels of approximation [7,8]. A standard approach used in continuum plasticity is the kinematic hardening model in which a single internal state variable called backstress accounts for the effect of variety of individual internal stresses. In this approach, the yield function $f(\boldsymbol{\sigma})$, where $\boldsymbol{\sigma}$ is the stress tensor, becomes $f(\boldsymbol{\sigma}-\boldsymbol{\sigma}_b)$ with $\boldsymbol{\sigma}_b$ being the backstress tensor [9]. The evolving backstress opposes the deformation during prestrain, and favors it upon load reversal. The above mentioned experimental studies have been used to estimate the magnitude of backstress and to assess the kinematic hardening behavior in plastically deformed Zirconium alloys [1,2,4–6]. Several continuum plasticity models with kinematic hardening were fitted to experimental data [4,6,10,11]. These models are typically full fledged, 3-dimensional, mostly anisotropic, complex phenomenological formulations with internal variables, set up in the framework of continuum viscoplasticity [9].

* Corresponding author.
E-mail address: radan.sedlacek@areva.com (R. Sedláček).

[1] In general, any deformation incompatibility causes internal stress. In Zirconium alloys, other possible sources of strain incompatibilities like second phase particles or dislocation cells/subgrains play probably only a secondary role [1,2].

http://dx.doi.org/10.1016/j.jnucmat.2016.07.025
0022-3115/

They are able to describe the material behavior in wide range of deformation conditions, including plasticity, cycling, creep and relaxation, but are generally deemed to be too complex, and the necessary fitting of the many parameters too costly, for practical engineering applications.

A different approach has been pursued in a wide class of studies focused on cladding creep behavior with practical applications in mind [12–20]. The proposed models describe the secondary (steady state) and primary (transient) creep strains as additive contributions. In a creep test at constant applied stress, the steady state creep rate is time independent, whereas the transient creep strain increases with time at a decreasing pace, finally reaching a saturated transient creep strain. The decreasing primary creep strain rate corresponds to a hardening. The hardening can be interpreted as time dependent or strain dependent. The latter appears to be the natural choice for simulation of creep curves[2] [12]. The strain hardening laws reportedly fail to describe the transient creep deformation following load drops and stress reversals. It was observed that just after a stress reversal, the material deformed as if it had not hardened before [15]. It was noted that a recovery of creep deformation in cladding tube samples depressurized after testing (i.e. stress removal) would occur if the cooling down was not quick enough [19]. The creep transients following stress drops could not be correctly described by a strain hardening law alone [20]. To cure the problem, quite complicated, ad hoc concepts of "recoverable hardening" [15] or time-dependent recoverable deformation ("anelastic strain") [12,20] were introduced, in addition to the primary and secondary creep contributions. Another approach motivated by the alleged inability of strain hardening to reproduce transient creep following stress drops and stress reversals utilizes the concept of viscoelasticity borrowed from the physics of polymers [24–26]. All these approaches were justified mostly by their ability to mathematically describe the measured creep transients following stress drops and stress reversals, whereas their physical interpretation was typically rather vague.

We note that in the discussions about the ability or not of a strain hardening law to describe transient creep of Zirconium alloys under varying stress conditions correctly, the *isotropic* strain hardening was always implicitly assumed. Then, it could be claimed that stress reversal and stress reduction are special situations where the hardening laws fail [24]. The purpose of this work is to show that introduction of a standard *kinematic* strain hardening model into a simple viscoplastic formulation enables us to account for the typical creep transients following stress drop, stress reversal, and stress removal quite satisfactorily while still staying within the framework of standard viscoplasticity of crystalline solids.

The plan of the paper is as follows. Dedicated creep tests with stress reversal and stress removal performed on Zircaloy cladding tube specimens are presented in Sec. 2. A simple viscoplastic model featuring mixed (i.e. isotropic and kinematic) strain hardening is developed in Sec. 3 and applied to simulation of creep tests with stress changes in Sec. 4. Discussion and conclusions follow in Secs. 5 and 6, respectively. The present paper is restricted to thermal creep of unirradiated Zircaloy.

2. Creep tests with stress reversal

2.1. Creep specimens and test conditions

The creep specimens have been fabricated from a cold worked and stress relieved Zircaloy-2 cladding tube that was manufactured in a standard mass production process. The finished specimens are helium filled, gas-tight welded pressurized tubes, their length being about ten times their diameter.

The gas pressure at the fill (i.e. room) temperature was calculated so that the nominal stress $\sigma = \sigma_\theta - \sigma_r$ (hoop minus radial stress component) at the test temperature 380 °C and atmospheric ambient pressure equals 75 MPa. The gas filled specimens were deformed in furnace (internal pressure) and in autoclave (outer overpressure). The pressure in the autoclave was set so that the resulting overpressure on the specimens caused the nominal stress $\sigma = \sigma_\theta - \sigma_r = -75$ MPa at the test temperature 380 °C. The samples were periodically removed after each 7 days of ageing in furnace or autoclave to measure the outer diameter. More detailed information on the creep specimens and tests parameters can be found in Appendix A.

2.2. Experimental program

The whole program included 8 creep specimens and can be seen at a glance in Fig. 1. The samples' denotation reflects the sequence of deformation conditions: F furnace, A autoclave, X creep collapse, 0 ageing at zero stress. At the beginning, four samples were deformed in furnace (380 °C, 75 MPa) and four in autoclave (380 °C, −75 MPa). One of the autoclaved samples (AXXX) underwent creep collapse after day 28. After 35 days of ageing, two samples were moved from furnace to autoclave (FAA0, FAF0) and two from autoclave to furnace (AFF0, AFAX). One sample continued to be deformed in the autoclave (to collapse after day 42, AAXX) and two in the furnace (FFF0, FFA0). The next change occurred after in total 56 days of ageing and the fate of the samples can be read out from their denotation and Fig. 1. After 84 days of deformation, all samples were placed into the autoclave where the pressure was set so as to balance their inner pressure at the test temperature 380 °C. That means the creep deformation from day 84 on occurred at zero applied stress.

2.3. Results

The most striking results are

- an increase in creep strain rate magnitude upon stress reversal
- a reversal of creep strain rate upon stress removal

Both can be seen clearly in Figs. 2 and 3. The former shows the accumulated creep strain

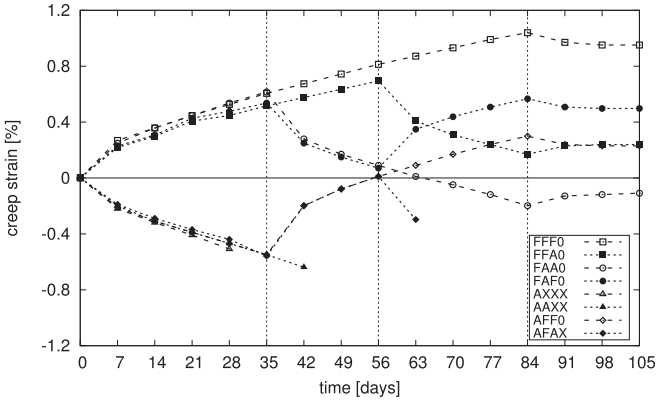

Fig. 1. Creep strain as function of time for all creep samples.

[2] The strain hardening concept has also been utilized in another class of cladding creep models for dry storage applications [21–23].

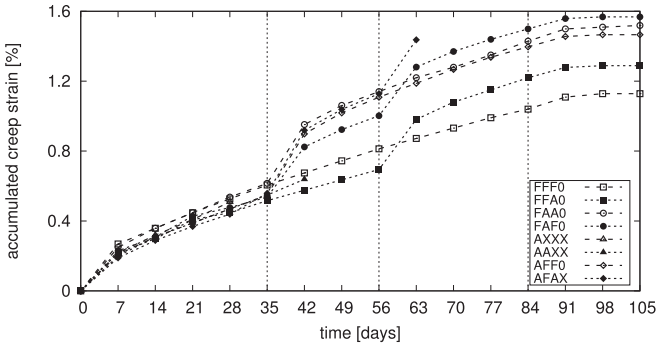

Fig. 2. Accumulated creep strain as function of time for all creep samples.

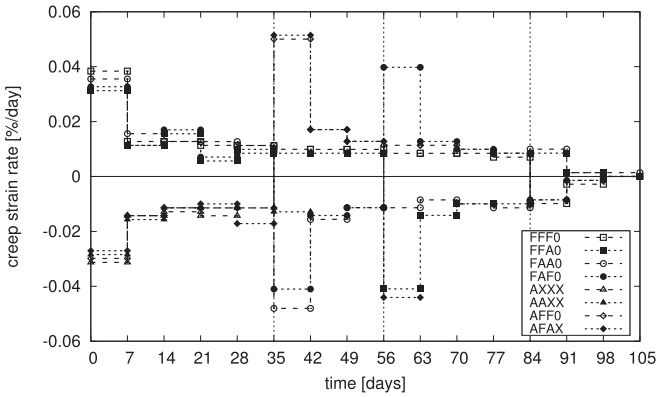

Fig. 3. Creep strain rate as function of time for all creep samples.

$$\varepsilon_{\mathrm{acc},I} = \sum_{i}^{I} \left| \Delta\varepsilon_i \right| \tag{1}$$

i.e. the sum of the strain increment magnitudes, as function of time. The latter displays the creep strain rate averaged over the $\Delta t = 7$ days periods between the diameter measurements

$$\bar{\dot{\varepsilon}}_i = \frac{\Delta\varepsilon_i}{\Delta t} \tag{2}$$

as function of time.

We observe a standard creep hardening behavior in the initial 35 days. The creep rate magnitude decreases at a decreasing pace. There is no systematic asymmetry between the loading in tension (furnace, F, inner pressure) and compression (autoclave, A, outer overpressure). The creep collapse (X) of some of the autoclaved samples will be discussed in Appendix B, in relation to the samples' ovality development.

After day 35, the creep strain rate of the samples that did *not* change their environment (FFF0, FFA0, AAXX) did not change either, or, perhaps, was still slightly decreasing. On the other hand, the creep strain rate of the samples that *did* change their environment (FAA0, FAF0, AFF0, AFAX) changed the sign and substantially increased in magnitude. The strain rate magnitude after the stress reversal was even larger than that of the virgin material at the test beginning. After that, the strain rate decreased again gradually.

After day 56, three samples continued to deform in their current environments (FFF0, FAA0, AFF0), their creep rate being either nearly steady state or still slightly decreasing. The other three samples changed their environment (FFA0, FAF0, AFAX). The corresponding increase in their creep strain rate magnitude was comparable to that observed after the first change of environment at day 35, obviously quite independent of their previous load history, i.e. with (FAF0, AFAX) or without (FFA0) a previous change of the environment.

From day 84 on, all the remaining samples were aged in the autoclave at zero applied stress. Immediately after the stress removal, one observes continuing creep deformation at approximately the same strain rate magnitude, however, in the opposite direction. Afterwards, the creep rate gradually decreases to zero.

3. Mixed hardening viscoplastic model

We consider a simple Hollomon-type viscoplastic constitutive law that reasonably represents the hardening behavior of metals and alloys under uni-directional, non-decreasing strain conditions, i.e. $\dot{\varepsilon} \geq 0$,

$$\sigma = K\varepsilon^n \dot{\varepsilon}^m \tag{3}$$

where K is a strength coefficient, n strain hardening coefficient, and m strain rate sensitivity exponent [9]. For practical applications, the model parameters K, n, and m can be rather complex functions of temperature, strain rate, cold work, irradiation, etc. [27]. For the present work, it is sufficient to treat these coefficients as constant numbers.

The model equation can be inverted to yield the creep strain rate $\dot{\varepsilon}$ as a function of the applied stress σ, and formally enhanced to get rid of the non-decreasing strain condition

$$\dot{\varepsilon} = \mathrm{sgn}(\sigma)\left(\frac{|\sigma|}{K\varepsilon_{\mathrm{acc}}^n}\right)^{1/m} \tag{4}$$

In this way, the accumulated creep strain $\varepsilon_{\mathrm{acc}}$ becomes an internal state variable responsible for the *isotropic* strain hardening. The evolution equation for the accumulated strain that corresponds to eq. (1) is

$$\dot{\varepsilon}_{\mathrm{acc}} = |\dot{\varepsilon}| \tag{5}$$

It is obvious that the response of this model to load reversal or load removal will not be correct: There will be certainly no increase in creep strain rate magnitude upon stress reversal and no creep rate at all at stress removal. Therefore, we introduce an additional internal state variable called backstress, σ_{b}, that accounts for the *kinematic* strain hardening

$$\dot{\varepsilon} = \mathrm{sgn}(\sigma - \sigma_{\mathrm{b}})\left(\frac{|\sigma - \sigma_{\mathrm{b}}|}{K\varepsilon_{\mathrm{acc}}^n}\right)^{1/m} \tag{6}$$

We choose the classical Armstrong-Frederic nonlinear kinematic hardening law [9] as evolution equation for the backstress

$$\dot{\sigma}_{\mathrm{b}} = H\dot{\varepsilon} - Q|\dot{\varepsilon}|\sigma_{\mathrm{b}} \tag{7}$$

In general, H is responsible for the increase in the incompatibility stress with strain and scales with elastic modulus, Q determines the dynamic strain relaxation of the incompatibility stress and is a function of temperature. In the present work, the coefficients H and Q are treated as simple parameters. Note that we have introduced the backstress pragmatically at the scalar level, rather than as a tensor which is the usual approach in the full fledged continuum viscoplasticity [9].

The internal state variables $\varepsilon_{\mathrm{acc}}$ and σ_{b} describe the state of the deforming material, whereas the difference between the applied stress and backstress, $\sigma - \sigma_{\mathrm{b}}$, has become the deformation driving

stress. The model defined by the system of ordinary differential equations (5)–(7) is a mixed (i.e. isotropic and kinematic) strain hardening, viscoplastic constitutive law that can be applied to simulation of creep and plasticity under varying loading conditions, including stress drops, stress removals and stress reversals.

4. Simulation of creep tests with stress changes

The purpose of this section is first of all to show the qualitative change in the model behavior induced by the kinematic hardening (as compared to the isotropic one) and to understand the role played by the backstress. The present simple model has neither the capability nor an ambition to describe the results of creep tests exactly.

The model defined by eqs. (5)–(7), must be supplemented by initial conditions. To start the simulations consistently, with practically zero strains and with zero backstress, and to avoid division by zero at the same time, we have used

$$\begin{array}{rcccl} \varepsilon_{\mathrm{acc}} & = & 10^{-9} & \text{for} & t=0 \\ \varepsilon & = & \mathrm{sgn}(\sigma)10^{-9} & \text{for} & t=0 \\ \sigma_{\mathrm{b}} & = & 0 & \text{for} & t=0 \end{array} \tag{8}$$

for simulation of all the creep tests in this work.

Based on the published assessments of backstress in Zircaloy [1,2,4–6], we have estimated the saturated backstress to be one half of the applied stress. This results in a relation between the coefficients of the kinematic hardening law (7), namely

$$H = Q\frac{|\sigma|}{2} \tag{9}$$

For comparison, the predictions of the isotropic hardening model, eqs. (4) and (5), complemented by the first two initial conditions (8), are also presented in the diagrams below. The model parameters have been fitted to the measured data so that the isotropic hardening model roughly describes the creep curves up to a first stress change, whereas the response of the mixed hardening model represents the complete measured creep strains as function of time.

4.1. Creep tests from Sec. 2

The model parameter values fitted to the experimental data are given in Table 1. The simulation results are described in the following.

Fig. 4 shows the creep test FFF0 that was conducted for 84 days in the furnace, unloaded, and further aged for the next 21 days. The creep rate up to the stress removal is reasonably well described by both models. The isotropic hardening model predicts no creep rate after the stress removal. The buildup of backstress in the mixed hardening model can be deduced from the upper part of Fig. 4: starting from zero, eq. (8), it saturates at $\sigma/2$, eqs. (7) and (9). The backstress contributes to hardening in the loaded part of the test, and drives the deformation in the opposite direction after the applied stress removal. The deformation driving stress $\sigma - \sigma_{\mathrm{b}}$ immediately before the unloading is $\sigma/2$, immediately after $-\sigma/2$.

Table 1
Model parameter values for simulation of the creep tests from Sec. 2, valid for ε in % and $\dot{\varepsilon}$ in %/day.

	K [MPa]	n [-]	m [-]	Q [-]	H [MPa]
isotropic hardening model	410	0.23	0.35	–	–
mixed hardening model	250	0.08	0.40	6	eq. (9)

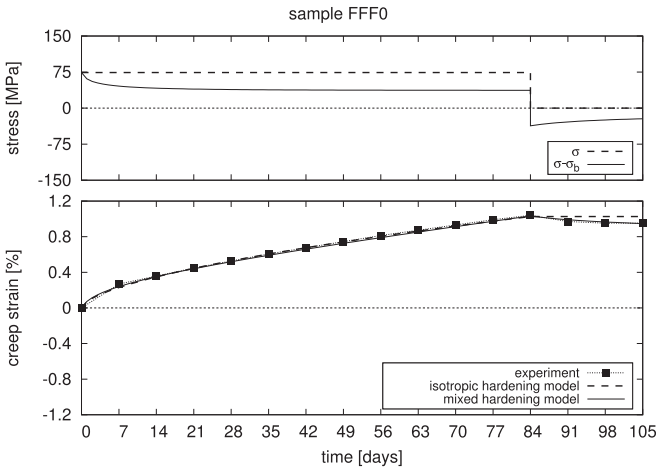

Fig. 4. Sample FFF0.

The creep strain rate thus reverses sign and keeps its magnitude upon the unloading, then the backstress declines, as it homes in on its new saturation value, i.e. zero. The creep strain rate declines with it, in accordance with the experimental data.

The other tests are concerned with stress reversals, always followed by the stress removal at day 84. Let us consider the test FFA0, Fig. 5, conducted for 56 days in the furnace, the next 28 days in the autoclave (stress reversal), and from day 84 on at zero applied stress. First of all, we note that the sample FFA0 creeps more slowly compared to the previous one, FFF0, cf. Figs. 1–3, for whatever reason (cf. Appendix A). Since the model parameter values have been fitted only once for the simulation of the whole test series, we cannot expect an exact reproduction of all the test results. Nevertheless, the difference in the response of the isotropic and mixed hardening models is obvious. The creep strain rate in the isotropic hardening model changes sign but not magnitude at the stress reversal. The creep continues with the same slowly decreasing rate. On the other hand, the sign changes and the strain rate magnitude increases dramatically in the mixed hardening model response. The deformation driving stress $\sigma - \sigma_{\mathrm{b}}$ immediately before the applied stress reversal is $\sigma/2$, immediately after $-3\sigma/2$. The negative peak in the $\sigma - \sigma_{\mathrm{b}}$ plot in the upper part of Fig. 5 clearly shows the short period where the backstress favors the deformation before falling back to contribute to hardening again. After the stress reversal, the

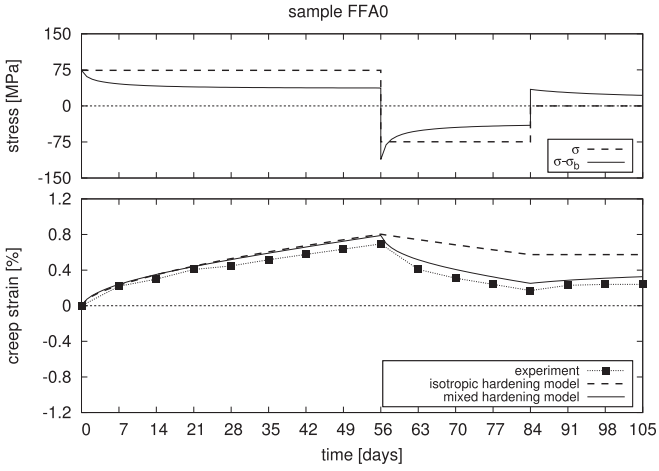

Fig. 5. Sample FFA0.

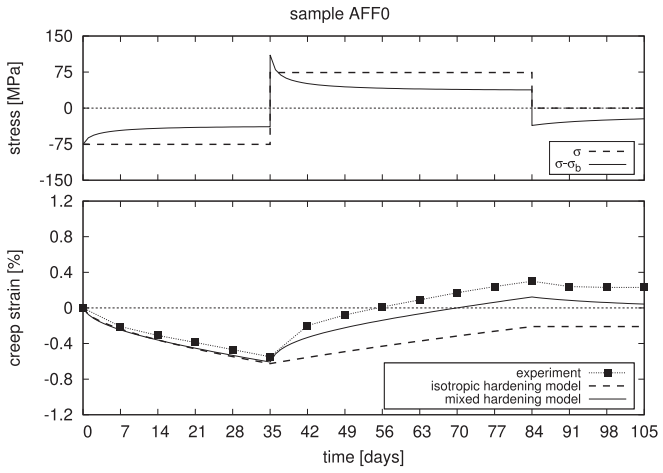

Fig. 6. Sample AFF0.

backstress declines from its positive $\sigma/2$ value. While passing zero, its effect switches from accelerating to decelerating. Then it approaches the negative $\sigma/2$ saturation value. The stress removal at day 84 follows the scenario described above (FFF0), but with the opposite sign.

The remaining tests are just variations on the same theme, see Figs. 6–11. The creep transients following the stress reversals are always very similar, independent of the specific initial situation. This means that even the shortest period of 21 days between the stress changes, see AFAX, Fig. 9, and FAF0, Fig. 10, is sufficient for the backstress to approach its saturation value and cause the creep acceleration after the stress reversal. Moreover, the creep behavior is quite symmetric relative to tension (furnace) and compression (autoclave). This is emphasized in Figs. 8 and 11 where the tests symmetric to each other are plotted in terms of accumulated creep strain versus time. In these figures, the creep acceleration following the stress reversals and correctly reproduced by the mixed hardening model can be clearly seen, as well as the inadequate behavior of the isotropic hardening model.

4.2. Creep tests performed by Matsuo [15]

Matsuo published results of a series of biaxial creep tests with stress and temperature changes on cold-worked and stress-relieved Zircaloy-4 cladding tube samples [15]. We apply the model developed in Sec. 3 to the stress change tests that were all conducted at the temperature of approximately 664 K. The model parameter values were fitted to the experimental data and are given in Table 2. The prediction of the isotropic hardening model has been plotted in the diagrams for comparison.

Fig. 12 shows a creep test featuring stress increase from 78 MPa to 148 MPa. The isotropic hardening model performs well in this case, the response of the mixed one is acceptable for the present purpose.

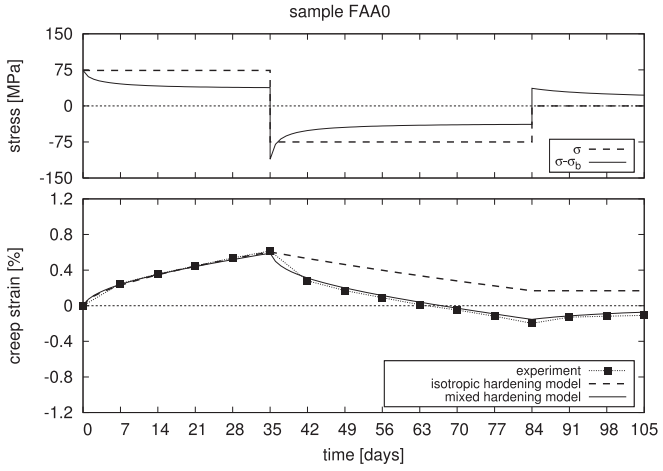

Fig. 7. Sample FAA0.

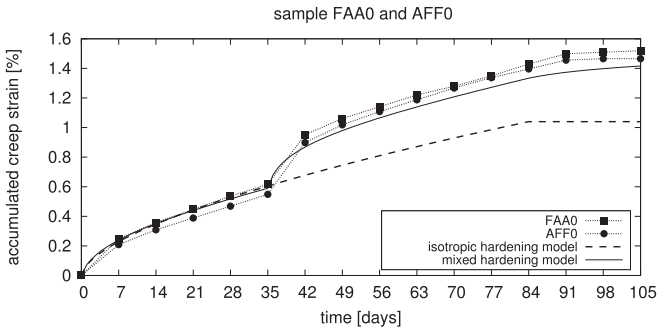

Fig. 8. Samples FAA0 and AFF0.

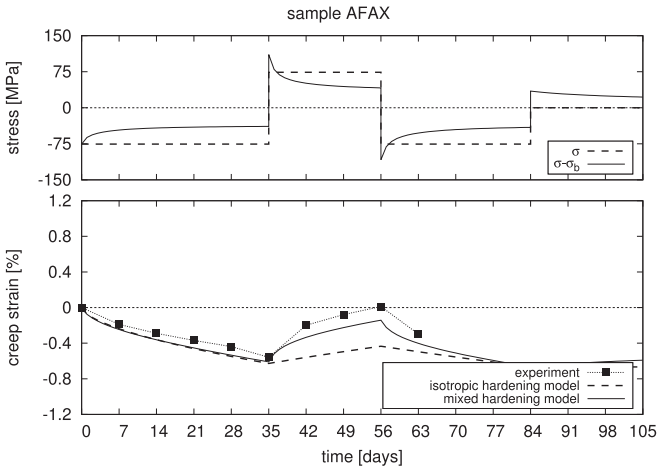

Fig. 9. Sample AFAX.

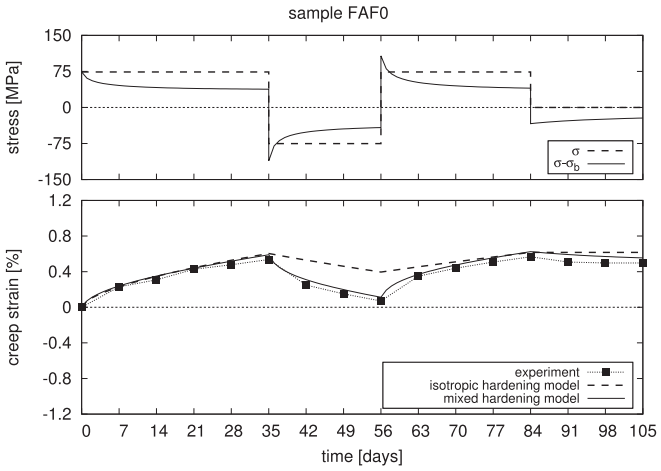

Fig. 10. Sample FAF0.

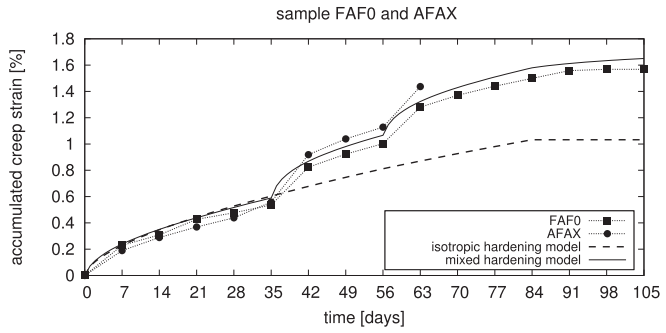

Fig. 11. Samples FAF0 and AFAX.

Table 2
Model parameter values for simulation of the creep tests of Matsuo [15], valid for ε in % and $\dot{\varepsilon}$ in %/day.

	K [MPa]	n [-]	m [-]	Q [-]	H [MPa]
isotropic hardening model	285	0.236	0.240	–	–
mixed hardening model	145	0.07	0.25	6	eq. (9)

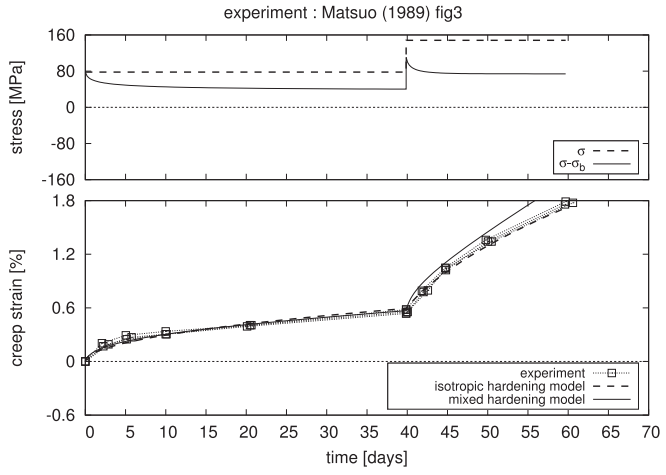

Fig. 12. Data from Matsuo [15], Fig. 3.

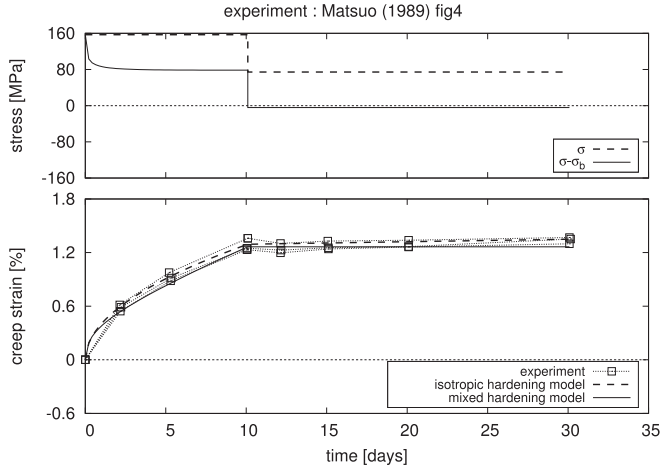

Fig. 13. Data from Matsuo [15], Fig. 4.

Fig. 13 displays a stress reduction from 157 MPa to 74 MPa. This test resembles a stress-dip test used to determine the internal backstress: at a stress reduction such that the applied stress after the reduction equals the backstress buildup before, a vanishing initial creep rate would result. Due to static recovery, the hardness of the material would then decrease and the creep would slowly resume again. In the present mixed hardening model, the backstress just before the stress reduction saturated at $\sigma/2 = 78.5$ MPa, so that the deformation driving stress $\sigma - \sigma_b$ immediately after the reduction was −4.5 MPa, resulting in a small negative creep strain rate, in a qualitative agreement with the experiment. In the absence of any static recovery mechanism in the present simple model, the resumption of positive strain rate observed in the experiment could not be reproduced. The isotropic strain hardening model yields a qualitatively wrong response, namely a mere reduction of the, still positive, strain rate.

Figs. 14 and 15 depict stress reversals. The former starting from 148 MPa, changing to −78 MPa and back to 147 MPa, the latter from 79 MPa to −118 MPa and back to 78 MPa. The simulation results are very similar to those in the previous Sec. 4.1, with the mixed hardening model performing quite well, the isotropic one being inadequate.

Finally, Fig. 16 represents several stress reversals between 148 MPa, −78 MPa and vice versa. It shows the limits of the current model formulation that has been reduced to an absolute minimum necessary to demonstrate the suitability of the kinematic hardening concept for simulation of the stress change tests. The simple model cannot cope with the repeated stress changes. Still reproducing the individual creep transients correctly, its global response gradually departures from the measured strain values.

5. Discussion

We have demonstrated that the transient creep behavior of Zircaloy related to stress reduction, stress removal, and stress reversal can be treated in the standard framework of continuum viscoplasticity with internal state variables by utilizing the kinematic strain hardening concept.

Alternative approaches suggesting recoverable [12,15,20] or anelastic strains [24–26] for the description of the creep transients are not necessary. For instance, the anelastic strain can be treated in the framework of viscoelasticity but is difficult to detect in real metals and alloys. The effects of partial recovery of plastic strain which typically justifies the introduction of anelasticity can be

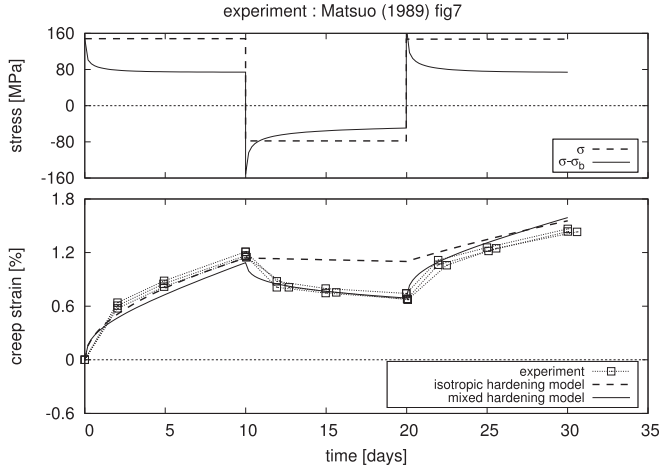

Fig. 14. Data from Matsuo [15], Fig. 7.

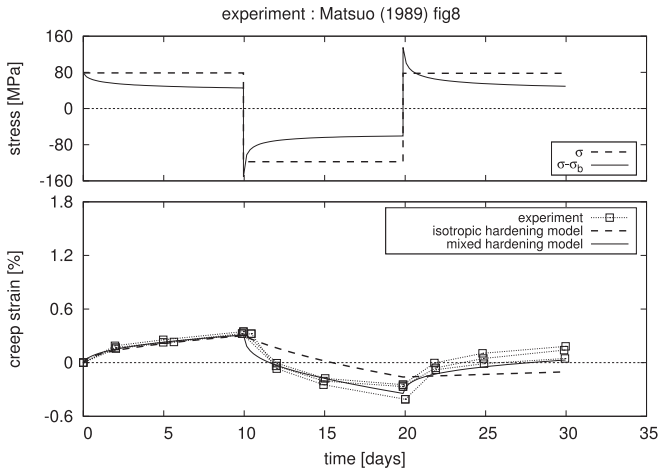

Fig. 15. Data from Matsuo [15], Fig. 8.

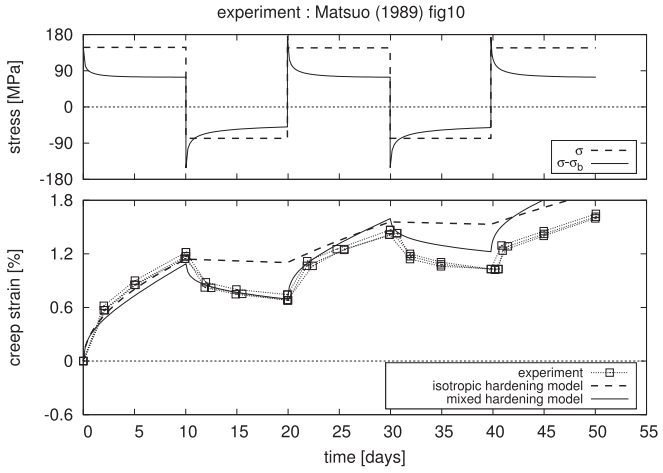

Fig. 16. Data from Matsuo [15], Fig. 10.

described within the scope of viscoplasticity by a proper choice of internal variables [9]. Also the time recovery effects that can be observed after unloading in creep of metals and alloys are well known and can be treated within the standard viscoplastic approach [9].

As explained in the Introduction, the macroscopic kinematic hardening concept is strongly backed not only by the ability of the existing models to describe the complex deformation behaviors of Zirconium alloys correctly [4,6,10,11], but also by the sound theoretical explanation considering the internal stress development at the microscopic level [2,7], by mathematical modeling of polycrystalline aggregates at the grain level [7,8], as well as by independent experiments, such as the in situ measurements of intergranular stresses [7], to cite just a few papers dealing directly with Zirconium alloys.

Another argument in favor of the kinematic hardening approach can be found in the dislocation-based modeling of plastic deformation of Zircaloy-4 [28]. The basis is the classical Kocks-Mecking model that accounts for the isotropic hardening due to dislocation density via the Taylor relation. Since the dislocation density is accessible to experimental measurements, the fitting of the model parameters is not so free as in purely phenomenological models. It appears that the isotropic, dislocation density induced, hardening alone cannot explain the observed hardening behavior of Zircaloy and an additional contribution is required. Although stress changes in creep were not in the focus of the work [28], the kinematic hardening has been introduced in the Kocks-Mecking model. The theoretical reasoning in favor of the existence of backstress in the hexagonal metal in Ref. [28] was standard, quite similar to ours (Sec. 1). We note in passing that the backstress in Ref. [28] was also introduced pragmatically at the scalar level.

The model developed in Sec. 3 was reduced to an absolute minimum necessary to demonstrate the suitability of the kinematic hardening concept for simulation of stress change tests. It has neither the capability nor an ambition to describe the results of creep tests exactly. This demonstrator model is not reasonably applicable to joint simulation of deformation under various loading conditions, e.g. creep and relaxation. For practical applications, a more sophisticated viscoplastic formulation would be required. Nevertheless, the present work demonstrates that, by utilizing the kinematic strain hardening concept and internal state variables, a simple and correct description of the creep transients following stress drops, stress reversals, and stress removals is possible within the standard viscoplastic approach.

6. Conclusions

- Results of biaxial creep tests with stress reversals and stress removals on Zircaloy-2 tube samples were presented.
- A simple Hollomon-type viscoplastic strain hardening model was extended by the Armstrong-Frederic nonlinear kinematic hardening law, resulting in a mixed (i.e. *isotropic* and *kinematic*) strain hardening model with internal state variables *accumulated creep strain* and *backstress*.
- The creep tests with stress changes described above as well as similar tests published in the literature were simulated by the isotropic as well as mixed hardening model.
- It was shown that introduction of the kinematic strain hardening in the viscoplastic model is sufficient to describe the creep transients following stress drops, stress reversals and stress removals correctly.
- Limits of the simplified approach used here to demonstrate the suitability of the kinematic strain hardening for simulation of the creep transients were discussed.

Acknowledgement

Thanks are due to Mr. G. Klose and his Measurement Lab Team for careful execution of the experiments.

A Creep specimens and tests conditions in detail

The nominal outer diameter of the cladding samples is $d_o = 10.050$ mm, the wall thickness $w = 0.605$ mm, so that validity of the thin wall approximation for evaluation of stress state in the closed pressurized tube can be assumed. The stress state “far enough” from the sample’s ends is assumed to be the one of an infinitely long closed tube exposed to inner and outer pressure, namely the nonvanishing principal stresses only: hoop, σ_θ, radial, σ_r, and axial, σ_a.

We use the stress difference $\sigma = \sigma_\theta - \sigma_r$ (hoop minus radial stress component, that is twice the maximum principal shear stress) as the measure of stress applied in the creep tests. The von Mises equivalent stress - which is typically considered to be the measure of deformation driving stress in many creep models - is directly related to this stress difference

$$\sigma_{vM} = \frac{\sqrt{3}}{2} \left| \sigma_\theta - \sigma_r \right| \tag{A1}$$

The stress difference $\sigma_\theta - \sigma_r$ can be evaluated in thin wall approximation, or alternatively, with the same result, from the exact elastic solution averaged over the wall thickness, as

$$\sigma_\theta - \sigma_r = \frac{2 r_i r_o (p_i - p_o)}{r_o^2 - r_i^2} \tag{A2}$$

where $r_o = d_o/2$, $r_i = (d_o - 2w)/2$ and p_o and p_i are the outer and inner pressure, respectively. We note that the hoop stress evaluated in thin wall approximation at mid radius $r = (r_i + r_o)/2$

$$\sigma_{\theta|_r} = \frac{r(p_i - p_o)}{w} \tag{A3}$$

attains values close to the stress difference (A2), cf. Table 3. The test stress and temperature were chosen in the scope given by the capability of the experimental devices so that a measurable creep deformation could be reached in reasonable times.

Table 3
Calculated pressures and stresses at the test temperature 380 °C.

	p_i	p_o	$\sigma_\theta - \sigma_r$	$\sigma_{\theta\|_r}$	[MPa]
furnace	9.77	0.1	75.17	75.48	
autoclave	9.77	19.44	−75.17	−75.48	

The diameter measurement occurs in cold conditions, so that thermal strains do not enter the results. The outer diameter is measured by a laser profilometer on a helical scan along the sample length and averaged along the gauge length. The uncertainty in the diameter measurement is ±3 μ m. The wall thickness is measured at a tube's end by an incremental feeler along its circumference and averaged, the resulting uncertainty being ±2 μ m. The temperature uncertainty in the furnace is about ±4 K. The estimated resulting uncertainty in the stress adjustment for the samples deformed in the furnace is ±2.5 MPa and the stress virtually does not change in the course of a test since the deformation induced changes in the specimen geometry and inner pressure almost perfectly compensate each other. The uncertainty in the stress adjustment in the autoclave is maximally ±0.7 MPa, in temperature ±3 K. The uncertainties are probably responsible for the observed differences in the measured creep strains of the different samples at nominally the same conditions. Anyway, the accuracy of the stress and temperature adjustment is fully sufficient for the present purpose.

B Development of ovality and creep collapse

An interesting byproduct of the present diameter measurements on the helical scan, see Appendix A, is the evaluation of ovality development of the samples. The ovality can be defined as

$$O = \frac{d_{max} - d_{min}}{d_{avg}} \times 100 \quad [\%] \tag{B4}$$

where d_{max}, d_{min}, and d_{avg} are the maximum, minimum, and averaged diameter, respectively, on the gauge length. Fig. 17 shows that the ovality increases in the outer overpressure conditions (autoclave, A), and decreases in the inner pressure conditions (furnace, F). The overpressure can cause even a creep collapse (samples AXXX, AAXX, AFAX). A period of inner pressure that increases the roundness before or between a period of outer overpressure can delay (sample AFAX) or even prevent the collapse (samples FAA0, FAF0).

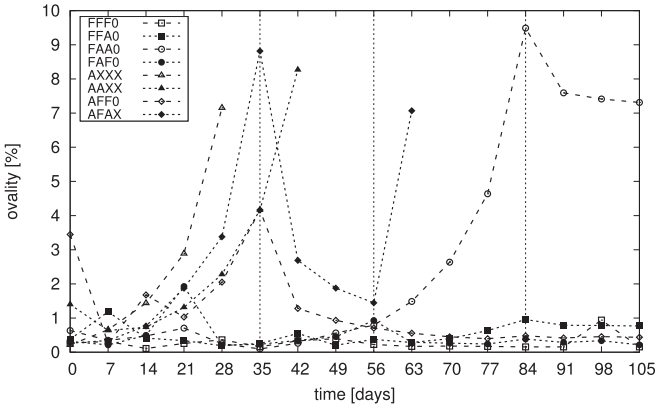

Fig. 17. Development of ovality for all creep samples.

References

[1] S.R. MacEwen, C.E. Ells, O.T. Woo, The Bauschinger effect in Zircaloy-2, J. Nucl. Mater. 101 (1981) 336–349.
[2] N. Christodoulou, Evolution of the Bauschinger effect in tension and compression in Zircaloy-2, Acta Metall. 37 (1989) 529–539.
[3] S.B. Wisner, M.B. Reynolds, R.B. Adamson, Fatigue behavior of irradiated and unirradiated Zircaloy and Zirconium, in: A.M. Garde, E.R. Bradley (Eds.), Zirconium in the Nuclear Industry: Tenth International Symposium, ASTM STP, vol. 1245, American Society for Testing and Materials, 1994, pp. 499–520.
[4] P. Delobelle, P. Robinet, P. Geyer, P. Bouffioux, A model to describe the anisotropic viscoplastic behaviour of Zircaloy-4 tubes, J. Nucl. Mater. 238 (1996) 135–162.
[5] C. Li, S. Ying, B. Shen, S. Qiu, X. Ling, Y. Wang, Q. Peng, Cyclic stress-strain response of textured Zircaloy-4, J. Nucl. Mater. 321 (2003) 60–69.
[6] F. Onimus, J.L. Béchade, C. Duguay, D. Gilbon, P. Pilvin, Investigation of neutron radiation effects on the mechanical behavior of recrystallized Zirconium alloys, J. Nucl. Mater. 358 (2006) 176–189.
[7] J.W.L. Pang, T.M. Holden, P.A. Turner, T.E. Mason, Intergranular stresses in Zircaloy-2 with rod texture, Acta Mater. 47 (1999) 373–383.
[8] F. Onimus, J.L. Béchade, A polycrystalline modeling of the mechanical behavior of neutron irradiated Zirconium alloys, J. Nucl. Mater. 384 (2009) 163–174.
[9] J. Lemaitre, J.L. Chaboche, Mechanics of Solid Materials, Cambridge University Press, Cambridge, 2000.
[10] F. Zaverl Jr., D. Lee, Constitutive relations for nuclear reactor core materials, J. Nucl. Mater. 75 (1978) 14–19.
[11] D. Lee, F. Zaverl Jr., E. Plaza-Meyer, Development of constitutive equations for nuclear reactor core materials, J. Nucl. Mater. 88 (1980) 104–110.
[12] K.L. Murty, K.K. Yoon, Creep transients in Zircaloy cladding, Scr. Metall. 13 (1979) 299–302.
[13] K.L. Murty, B.L. Adams, Biaxial creep of textured Zircaloy I: experimental and phenomenological descriptions, Mater. Sci. Eng. 70 (1985) 169–180.
[14] Y. Matsuo, Thermal creep of Zircaloy-4 cladding under internal pressure, J. Nucl. Sci. Technol. 24 (1987) 111–119.
[15] Y. Matsuo, Creep behavior of Zircaloy cladding under variable conditions, in: L.F.P. Van Swam, C.M. Eucken (Eds.), Zirconium in the Nuclear Industry: Eighth International Symposium, ASTM STP, vol. 1023, American Society for Testing and Materials, Philadelphia, 1989, pp. 678–691.
[16] M. Mayuzumi, T. Onchi, Creep deformation of an unirradiated Zircaloy nuclear fuel cladding tube under dry storage conditions, J. Nucl. Mater. 171 (1990) 381–388.
[17] M. Mayuzumi, T. Onchi, Creep deformation and rupture properties of unirradiated Zircaloy-4 nuclear fuel cladding tube at temperatures of 727 to 857 K, J. Nucl. Mater. 175 (1990) 135–142.
[18] M. Mayuzumi, T. Onchi, The applicability of the strain-hardening rule to creep deformation of Zircaloy fuel cladding tube under dry storage condition, J. Nucl. Mater. 178 (1991) 73–79.
[19] M. Limbäck, T. Andersson, A model for analysis of the effect of final annealing on in- and out-of-reactor creep behavior of Zircaloy cladding, in: E.R. Bradley, G.P. Sabol (Eds.), Zirconium in the Nuclear Industry: Eleventh International Symposium, ASTM STP, vol. 1295, American Society for Testing and Materials, 1996, pp. 448–468.
[20] K.L. Murty, Creep studies for Zircaloy life prediction in water reactors, JOM J. Minerals, Metals Mater. Soc. 9910 (1999) 32–39.
[21] R. Limon, C. Cappelaere, T. Bredel, P. Bouffioux, A formulation of the spent fuel cladding creep behaviour for long term storage, in: Proceedings of ANS International Topical Meeting on Light Water Reactor Fuel Performance, Park City, Utah, 2000.

[22] R. Limon, S. Lehmann, A creep rupture criterion for Zircaloy-4 fuel cladding under internal pressure, J. Nucl. Mater. 335 (2004) 322–334.
[23] C. Cappelaere, R. Limon, C. Duguay, G. Pinte, M. Le Breton, P. Bouffioux, V. Chabretou, A. Miquet, A robust model to describe the thermal creep of CWSR Zircaloy 4 cladding for fuel cycle back-end application, in: Proc. 2011 Water Reactor Fuel Performance Meeting, 2011 pages T4–005.
[24] V. Tulkki, T. Ikonen, Modeling of Zircaloy cladding primary creep during load drop and reversal, J. Nucl. Mater. 445 (2014) 98–103.
[25] V. Tulkki, T. Ikonen, Viscoelastic modeling of Zircaloy cladding in-pile transient creep, J. Nucl. Mater. 457 (2015) 324–329.
[26] V. Tulkki, T. Ikonen, Modelling anelastic contribution to nuclear fuel cladding creep and stress relaxation, J. Nucl. Mater. 465 (2015) 34–41.
[27] D.T. Hagrman, SCDAP/RELAP5/MOD3.1 Code Manual Volume IV: MATPRO – a Library of Materials Properties for Light-water-reactor Accident Analysis. NUREG/CR-6150 EGG-2720 Volume IV, Idaho National Engineering Laboratory, 1993.
[28] J.W. Dunlop, Y.J.M. Bréchet, L. Legras, Y. Estrin, Dislocation density-based modelling of plastic deformation of Zircaloy-4, Mater. Sci. Eng. A 443 (2007) 77–86.